crystals

MDPI

Article

Morphology Modification of Mg_2Si by Solution Treatment and Its Effects on the Mechanical Properties of TiB_2/Mg-4Al-1.5Si Composites

Jian Liu [1], Xiaogang Chen [2], Wuxiao Wang [2,*], Shaoyong Qin [2] and Haoran Xu [3]

[1] Faculty of Printing, Packaging Engineering and Digital Media Technology, Xi'an University of Technology, Xi'an 710054, China
[2] School of Material Science and Engineering, Xi'an University of Technology, Xi'an 710048, China
[3] Jiangsu Huayu Printing & Coating Equipment Co., Ltd., Nan Tong 226300, China
* Correspondence: wangwx@xaut.edu.cn

Abstract: TiB_2/Mg-4Al-1.5Si magnesium matrix composites were prepared by semi-solid stirring assisted ultrasonic treatment, the primary Mg_2Si phases in the composites exhibit polygon with sharp corners, and the eutectic Mg_2Si phases appear thin Chinese-script or short-strip shape. To reduce stress concentration around the sharp corners (tips) of the Mg_2Si phases, the morphology of the Mg_2Si phases was further modified by solution treatment at 420 °C for 24 h, and the effects of the morphology modification of the Mg_2Si phases on the mechanical properties of the composites were investigated. The results showed that after the solution treatment, the sharp corners of the primary Mg_2Si phases were blunted, and the partial branches of the eutectic Mg_2Si phases were dissolved into particles. The Vickers-hardness, ultimate tensile strength, yield strength, and elongation of the composites were increased by 11.50%, 33.28%, 28.57%, and 27.17% compared with those of unmodified composites, respectively. The solution treatment exhibits a more significant strengthening effect for the composites in hardness, ultimate tensile strength, and yield strength compared with the matrix alloys.

Keywords: magnesium matrix composites; Mg_2Si; solution treatment; mechanical properties

Citation: Liu, J.; Chen, X.; Wang, W.; Qin, S.; Xu, H. Morphology Modification of Mg_2Si by Solution Treatment and Its Effects on the Mechanical Properties of TiB_2/Mg-4Al-1.5Si Composites. *Crystals* **2022**, *12*, 1260. https://doi.org/10.3390/cryst12091260

Academic Editors: Ireneusz Zagórski, Mirosław Szala and Pavel Lukáč

Received: 14 August 2022
Accepted: 1 September 2022
Published: 5 September 2022

1. Introduction

As the lightest structural metal material, magnesium alloy has great prospects for application in the fields of automobile, aerospace, and weapon industry owing to its high specific strength and stiffness, low coefficient of thermal expansion, and good damping performance [1–3]. Mg-Al series alloys are the most commercially used magnesium alloys due to their good castability, high strength, and low price. However, the β-$Mg_{17}Al_{12}$ phase with a low melting point is easy to be softened and coarsened above 120 °C, thereby deteriorating the mechanical properties of the magnesium alloys and severely restricting their large-scale applications in medium-high temperature components [4,5]. To improve the strength of Mg-Al series alloys at room and elevated temperatures, several elements with low solid solubility in Mg-Al alloys (such as Ca, Si, Mn, rare earth elements, etc.) were added to form secondary phases with high thermal stability [6–8]. The intermetallic Mg_2Si phase has a high melting point (1085 °C), high hardness (4.5×10^9 N/m^2), high elastic modulus (120 GPa), low coefficient of thermal expansion (7.5×10^{-6} K^{-1}), and similar density to magnesium (1.99 g/cm^3), thus low-cost Mg-A1-Si series magnesium alloys are developed by adding Si to Mg-Al alloys [9,10]. The fine Mg_2Si phases dispersed at grain boundaries can hinder grain boundary sliding and improve strength. However, the eutectic Mg_2Si phases in as-cast Mg-Al-Si alloys generally exhibit undesirable coarse Chinese scripts, when the Si content is high, the coarse dendritic primary Mg_2Si phases will appear, split the matrix of Mg-Al-Si alloys, and break or debond under loading, thereby deteriorating the strength and ductility of the alloys [11–13]. Therefore, it is critical to refine

and modify the Mg_2Si phases for improving the comprehensive mechanical properties of Mg-Al-Si series magnesium alloys.

To refine the coarse Mg_2Si phases, various techniques have been developed and utilized, such as rapid solidification [14], ultrasonic treatment [15], and plastic deformation [16]. Among these methods, modification treatment by adding trace elements, modifiers of nucleation agents (Ce, Sr, Ca, Na, Li, P, Sb, Bi, and their combination, AlP, TiB_2, etc.) is a simple and cost-effective technique to refine and modify the coarse Mg_2Si during solidification process [17–21]. TiB_2 particles are not only one of the ideal reinforcements for Mg and Mg alloys, but also have been used as heterogeneous nuclei to refine the coarse Mg_2Si phases due to the good lattice matching coherence relationship between TiB_2 and Mg_2Si (the disregistry between the (0001) crystal plane of the TiB_2 and the (200) crystal plane of the Mg_2Si is 4.64%) [22–24]. In our previous study, TiB_2 particles were added to an Mg-4Al-1.5Si alloy melt by semi-solid stirring assisted ultrasonic vibration, and it was found that not only the coarse dendritic Mg_2Si phases and Chinese script-like eutectic Mg_2Si phases were significantly refined, but also the refined primary Mg_2Si particles were uniformly dispersed during solidification. However, the refined primary Mg_2Si particles in the composites exhibit polygonal shapes with sharp corners, and the eutectic Mg_2Si phases exhibit thin Chinese script or short rod shapes [25]. It is well known that fine and spherical particles have higher fracture stress and stronger particle/matrix interfacial bonding strength [26]. Hence, it is necessary to further refine the eutectic Mg_2Si phases and to passivate the primary Mg_2Si phases for improving their strengthening effect.

Research shows that the modification treatment followed by heat treatment can further enhance the strength of the alloy due to the spheroidizing and passivation phenomenon of the Mg_2Si phase during the heat treatment process [27–29]. Heat treatment is a low-cost and convenient method to modify the morphology of the Mg_2Si phase by the local dissolution of Mg_2Si via solid-diffusion of Si atoms at high temperatures [30–32]. Xu et al. [33] carried out solution treatment (at 545 °C for 4–8 h) and aging treatment (at 170 °C for 8 h) to an in-situ Mg_2Si reinforced Al-18%Si matrix composites, and found that the longer the solution time, the more dendrites were dissolved and passivated when treated for 8 h, the Mg_2Si phases were smaller, mostly granular and distributed uniformly, which improved the strength, hardness and wear resistance of the composites. Wang et al. [34] investigated the effect of solution treatment (at 420 °C for 10 h) and aging treatment (at 180 °C for 0–100 h) on the microstructure and mechanical properties of Mg-3Al-1Si-0.3Mn-xSr (x = 0, 0.2, 0.4) alloy, it was found that the dendrite of the eutectic Mg_2Si phases becomes narrower and thinner than the as-cast microstructure. After the aging treatment, the microstructure of the alloy had no obvious change, and the mechanical properties had a slight increase. Liu et al. [35] utilized solution treatment (at 420 °C for 4, 8, and 12 h) to modify the in-situ Mg_2Si in an Mg-5Si-0.5Y-0.5Sb foam, and found that the eutectic Mg_2Si phases were spheroidized, the corners of the primary Mg_2Si were passivated gradually with the increasing holding time of the solution heat treatment, and the compressive strength and energy absorption of the foams were improved consequently. However, there is little research on the effect of solution treatment on the morphology of Mg_2Si phases in hybrid reinforced Mg-Al-Si magnesium matrix composites.

In the present work, the effect of solution treatment on the morphology of Mg_2Si phases in TiB_2/Mg-4Al-1.5Si composites were investigated, and the modification effect of the composites was evaluated in terms of mechanical properties and compared with the Mg-4Al-1.5Si alloys treated under the same conditions.

2. Materials and Methods

The 3 vol.% TiB_2/Mg-4Al-1.5Si composites were fabricated by semi-solid stirring assisted ultrasonic treatment, and the semi-solid temperature was selected based on results from differential thermal analysis (DTA) on a thermal analyzer (STA 499 F3, NETZSCH). Figure 1 depicts the DTA profile of the as-cast Mg-4Al-1.5Si alloys, and it can be seen that there are three exothermic peaks, corresponding to the melting of ternary eutectic

α-Mg + $Mg_{17}Al_{12}$ + Mg_2Si (at 435.9 °C), binary eutectic α-Mg + Mg_2Si (at 585.5 °C), and primary Mg_2Si (at 640.4 °C) [17]. Hence, the stirring temperature was selected between 585.5 and 640.4 °C. Figure 2 illustrates the main two steps in fabricating the composites. After Mg-4Al-1.5Si magnesium alloy was melt completely at 720 °C, the melt was cooled to 635 °C in the semi-solid state, and 3 vol.% TiB_2 particles (with an average diameter of 50 nm, obtained from Shanghai Xiangtian Nanomaterials Co., Ltd. Shanghai, China.) preheated to 635 °C were added to the melt, while the melt was mechanically stirred at 600 rpm, thereby incorporating and dispersing the TiB_2 particles into the melt under its high viscous force in the semi-solid state. After the mechanical stirring for 5 min, the melt was reheated to 720 °C, and processed by supersonic treatment with a power of 1.8 kW and a frequency of 20 kHz. Under the acoustic cavitation and acoustic streaming induce by ultrasonic waves, the TiB_2 particles were further dispersed throughout the melt. After the supersonic treatment for 20 min, the mixed melt was poured into a cylindrical steel permanent mold. The melting, mechanical stirring, and ultrasonic treatment were carried out in an Argon atmosphere to prevent the burning of the alloy melt. The specimens for solution treatment were cut from the center of the obtained cast ingot 75 mm from the bottom. Solution treatment was carried out in a chambered resistance furnace (SX2-5-12A). Generally, the upper limit temperature of solution treatment is the incipient melting temperature of the low melting point phase, to prevent the partial remelting of the Mg-4Al-1.5Si alloy during the solution treatment, the solution temperature should be lower than the incipient melting temperature of the Mg-4Al-1.5Si alloy. According to the differential thermal analysis (DTA) profiles of the as-cast Mg-4Al-1.5Si alloys (see Figure 1), the incipient melting temperature of the alloys is 435.9 °C. By referring to other similar research [34,35], the solution conditions were selected as 420 °C for 24 h, followed by quenching in cold water. To prevent the oxidation of the composites during the heat treatment process, the specimens were covered by graphite powder.

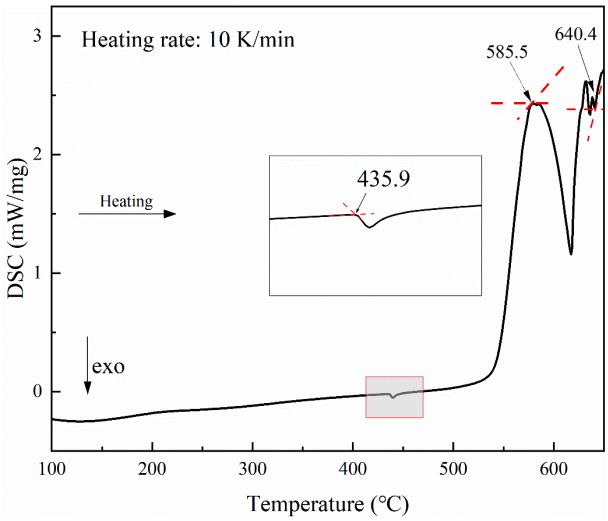

Figure 1. Differential thermal analysis (DTA) profiles of as-cast Mg-4Al-1.5Si alloy.

The as-cast and solution-treated specimens were ground, polished, and etched with acetic-picral reagent (5 mL acetic acid, 5 mL picric acid, 10 mL H_2O, and 100 mL ethanol) for 10−15 s, and the grain distribution was statistically measured by mean linear intercept method. The phase constituents of the as-cast composites were analyzed by XRD-7000 X-ray diffractometer (XRD) using Cu K_α radiation in step mode 20° to 90° with a scanning speed of 10°/min. The microstructures of the specimens were observed by using OLYMPUS GX71 optical microscope (OM), and the morphology of Mg_2Si in the composites was analyzed through a JSM-6700 F scanning electron microscope (SEM). The tensile test was conducted in the HT-2402 material testing machine without extensometer at a constant tensile speed of 0.8 mm/min at room temperature. Three specimens with dimensions of

15 mm length, 5 mm width, and 2 mm thickness in the gauge section were tested for each material to reduce the effect of random noise according to the ASTM-E8 standard. The Vickers hardness was determined on a Vickers hardness tester (HV-120) with a loading force of 5 kg for a dwell time of 15 s, and an average value was obtained through five tests at different positions on each specimen.

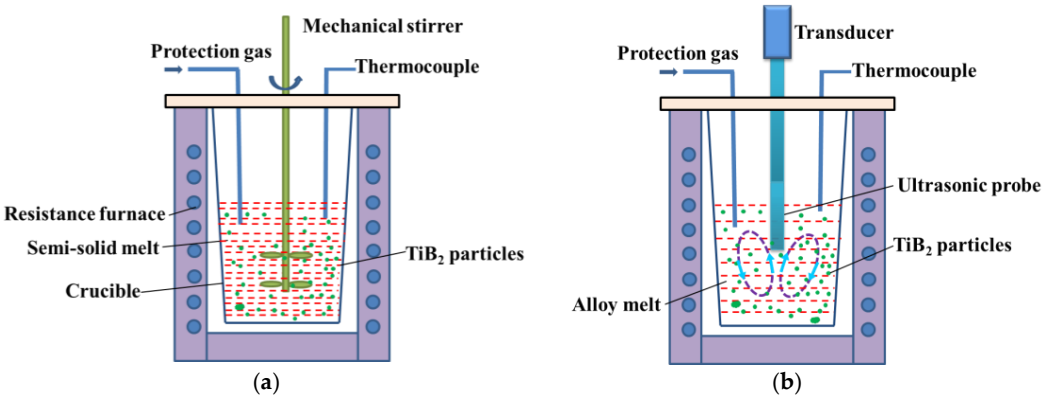

Figure 2. Schematic of the fabrication process of TiB_2/ Mg-4Al-1.5Si alloy composites, (**a**) mechanical stirring in semi-solid state, (**b**) ultrasonic treatment in the liquid state.

3. Results

3.1. Microstructure of the Composites

Figure 3 shows the optical microstructure of the as-cast and solution-treated TiB_2/Mg-4Al-1.5Si composites. Figure 4 shows the X-ray diffraction (XRD) pattern of the as-cast composites, it can be seen that α-Mg (2θ: 32.19–72.49°), β-$Mg_{17}Al_{12}$ (2θ: 24.78–69.35°), Mg_2Si (2θ: 33.93–70.18°), and TiB_2 (2θ: 68.13–78.64°) were detected, and the peaks corresponding to TiB_2 were not visible due to its relatively low content (3 vol.%). Hence, the microstructure of the as-cast TiB_2/Mg-4Al-1.5Si composites consist of α-Mg, a small amount of island-like β-$Mg_{17}Al_{12}$ phases at grain boundaries, polygonal primary Mg_2Si phases, thin Chinese script and short strip-shaped eutectic Mg_2Si phases (as shown in Figure 3a). After the solution treatment, the β-$Mg_{17}Al_{12}$ along the grain boundaries of the composites was dissolved almost completely, and the morphology and size of the primary Mg_2Si phases remained unchanged, but the corner became obtuse, partial branches of the eutectic Mg_2Si phases were decomposed into disconnected particles, as shown in Figure 3b).

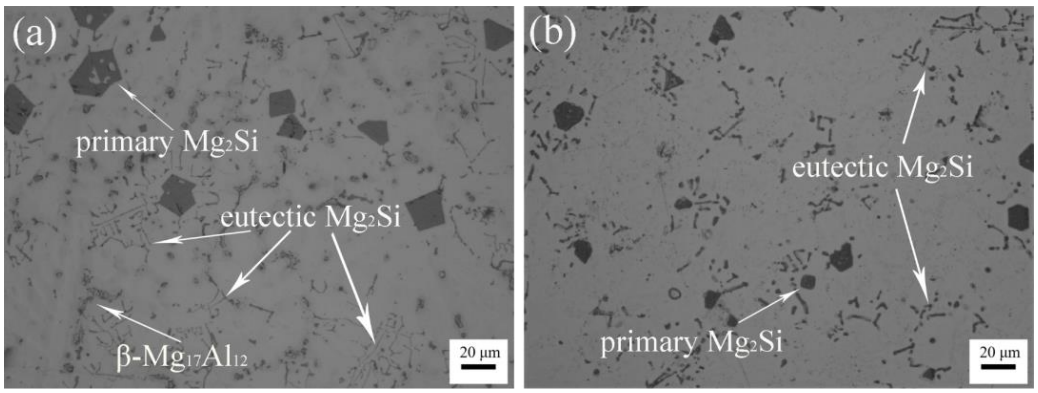

Figure 3. Optical microstructure of the as-cast composites (**a**); and solution-treated composites (**b**).

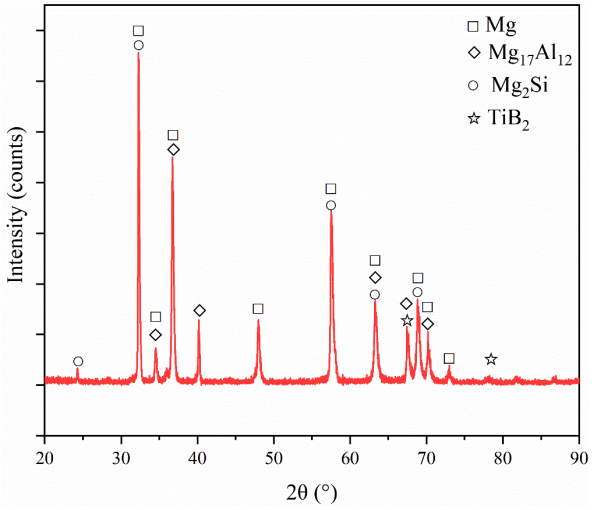

Figure 4. XRD patterns of the as-cast TiB_2/Mg-4Al-1.5Si composites.

Figure 5 shows the magnified SEM micrographs of the eutectic Mg_2Si phases in the TiB_2/Mg-4Al-1.5Si composites before and after the solution treatment. The eutectic Mg_2Si phases in the as-cast TiB_2/Mg-4Al-1.5Si exhibit Chinese script and short strip shape, and there exist concaves and convexities on their surface (as shown in Figure 5a). After solution treatment, partial branches of the eutectic Mg_2Si phases were transformed into fine dot-like particles (as shown in Figure 5b).

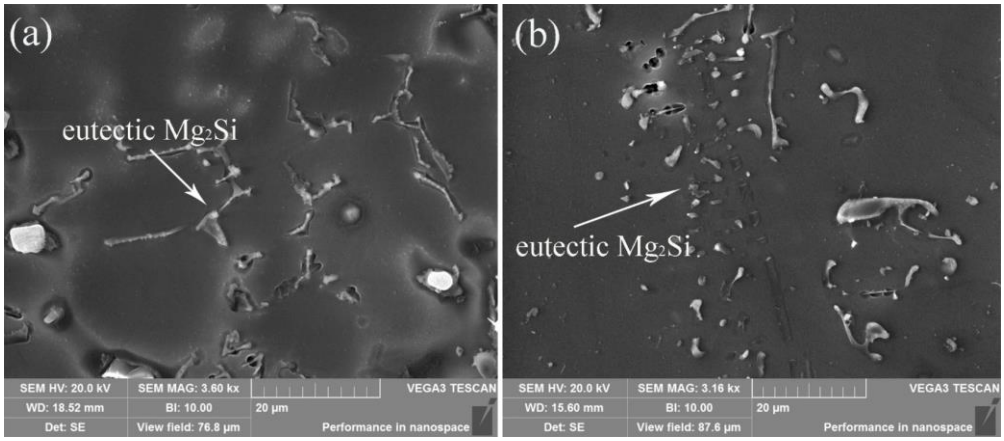

Figure 5. SEM micrographs of the eutectic Mg_2Si phases in the (**a**) as-cast composites; and (**b**) solution-treated composites.

Figure 6 shows the magnified SEM micrographs of the primary Mg_2Si phases in the TiB_2/Mg-4Al-1.5Si composites before and after solution treatment. As shown in Figure 6a, the primary Mg_2Si phases in the as-cast composites exhibit irregular polygons with sharp corners, and some eutectic Mg_2Si phases are connected with them or distributed around them. After solution treatment, the primary Mg_2Si is still irregular and polygon-like, but the sharp corners became obtuse, and the eutectic Mg_2Si phases connected with the primary Mg_2Si phases were dissolved, as shown in Figure 6b. It is concluded that solution treatment can contribute to the breakage of the eutectic Mg_2Si phases and can promote the passivation of the sharp corners of the primary Mg_2Si phases.

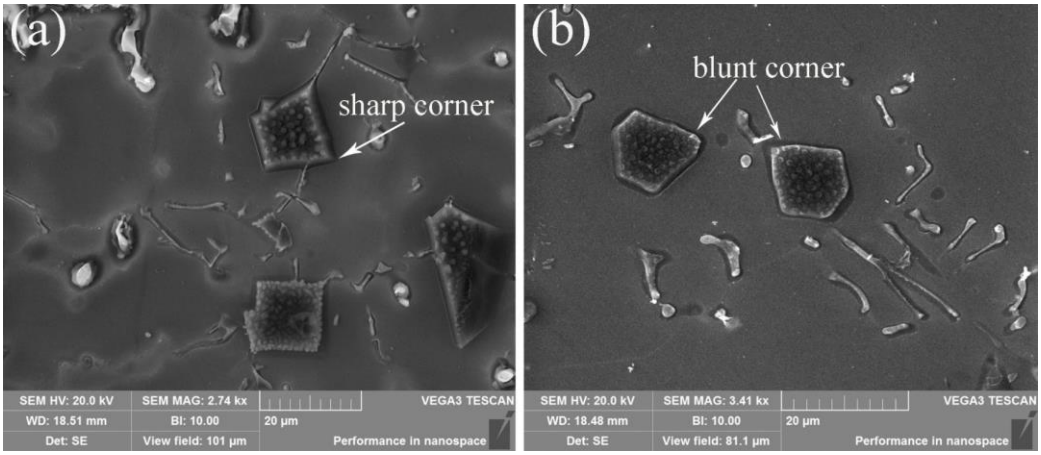

Figure 6. SEM micrographs of the primary Mg_2Si phases in the (**a**) as-cast composites and (**b**) solution-treated composites.

The solubility of Si in Mg is very limited, only about 0.003 at%, which indicates that it is difficult for Si to diffuse in Mg-Al-Si alloys [12]. However, in the process of solution treatment, the vibrational energy and diffusion coefficient of the atoms is improved at high temperatures, and it makes the Si short-circuit diffusion along the Mg_2Si/Mg interface easier [34]. The Mg_2Si/Mg interface plays an important role in the morphology changes of the Mg_2Si phases, and a rugged interface between the Mg_2Si phases and α-Mg matrix will cause microscopic stress, and the Si atoms will diffuse randomly along the Mg_2Si/Mg interface under the action of the microscopic stress [36]. Furthermore, the Mg_2Si/Mg interface generally contains lots of defects such as vacancies, dislocations, and sub-boundary, which can accelerate the diffusion of Si atoms along the Mg_2Si/Mg interface [34]. According to the Gibbs-Thomson formula [33], the concentration of Si in the Mg_2Si phases with large curvature can be expressed as:

$$\ln \frac{C_\alpha(r)}{C_\alpha(\infty)} = \frac{2\sigma V_B}{k_B T r} \quad (1)$$

where r is the curvature radius, $C_\alpha(r)$ is the concentration of Si at r, $C_\alpha(\infty)$ is the concentration of Si at the flat interface, σ is the surface tension, V_B is the volume of Si atom, T is the temperature, and k_B is the coefficient related to the shape. According to Equation (1), the Si concentration is higher at the Mg_2Si/Mg interface with a smaller curvature radius (i.e., greater curvature or convexity).

There are lots of concaves and convexities on the surfaces of the eutectic Mg_2Si phases along the Mg_2Si/Mg interface, as shown in Figure 5a. Due to the difference in curvature radius at these concaves and convexities, there exists a concentration gradient of Si along the Mg_2Si/Mg interface. During the solution treatment, the Si atom diffused from the Si enrich region (concave pit, sharp corner, or tip) to the Si poor region (flat interface) under the action of surface tension, hence the sharp corner of the Mg_2Si phases was partially melted, and some eutectic Mg_2Si phases were melted at pits or roots and transformed into particles. With the accumulation of Si at the flat interface, new fine Mg_2Si particles were precipitated and spheroidized [33]. Part of the eutectic Mg_2Si phases was not broken into particles and kept stable, as shown in Figure 5b, it may be ascribed to their relatively smooth surfaces, and the Si diffusion along the flat interface is homogeneous.

3.2. Mechanical Properties

Figure 7 shows the Vickers-hardness of the alloy and the composites in the as-cast state and after solution treatment. It is seen that the hardness of the alloy and composites after solution treatment is HV 60.3 and HV 126, respectively, which is 7.7% and 11.5% higher than that in the as-cast state. Figure 8 plots the typical engineering stress-strain

curves of the alloy and composites before and after solution treatment at room temperature, and the corresponding ultimate tensile strength (UTS), yield strength (YS), and elongation (EL) are listed in Figure 9 and Table 1. It can be seen that the UTS, YS, and EL of the solution-treated alloy were increased by 21.5%, 5.4%, and 37.5%, respectively compared with the as-cast alloy, while the UTS, YS, and EL of the composites were increased by 33.3%, 28.5%, and 27.2%, respectively compared with the as-cast composites. Hence, it is concluded that solution treatment was capable of improving the strength and ductility of the Mg-4Al-1.5Si alloy and TiB_2/Mg-4Al-1.5Si composites, and the strengthening effect of the solution treatment is more significant for the composites in terms of hardness, UTS, and YS.

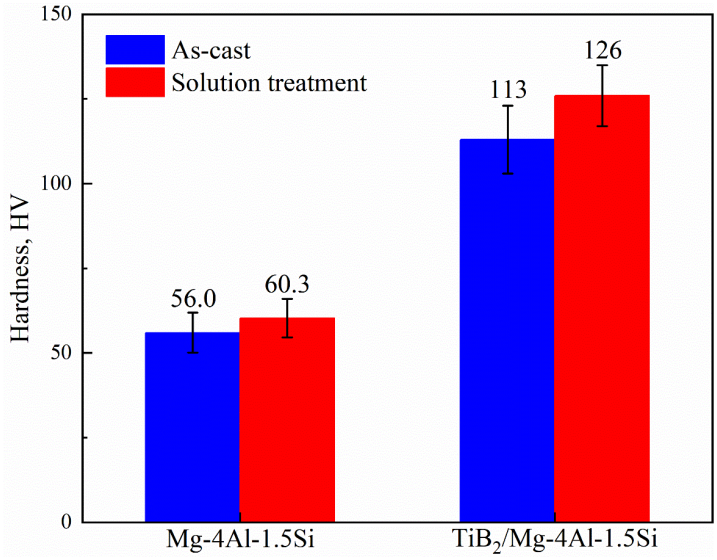

Figure 7. Vickers-hardness of the alloys and the composites in as-cast state and after solution treatment.

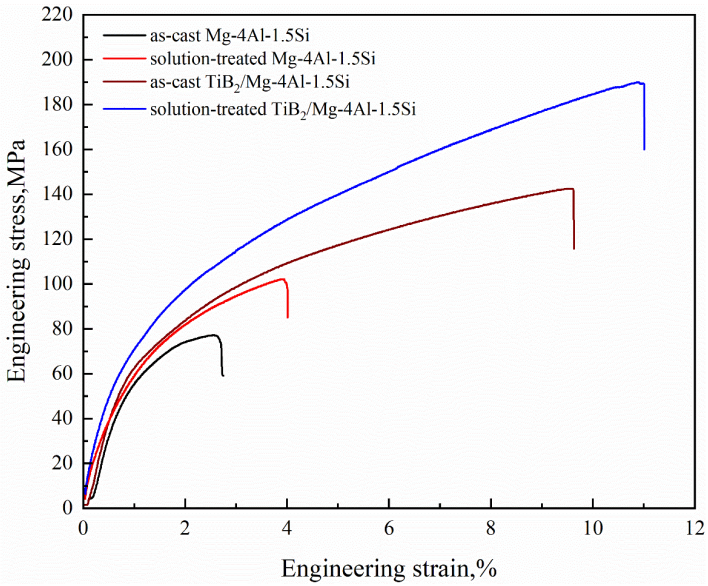

Figure 8. Typical tensile stress-strain curves of the alloys and the composites in as-cast state and after solution treatment.

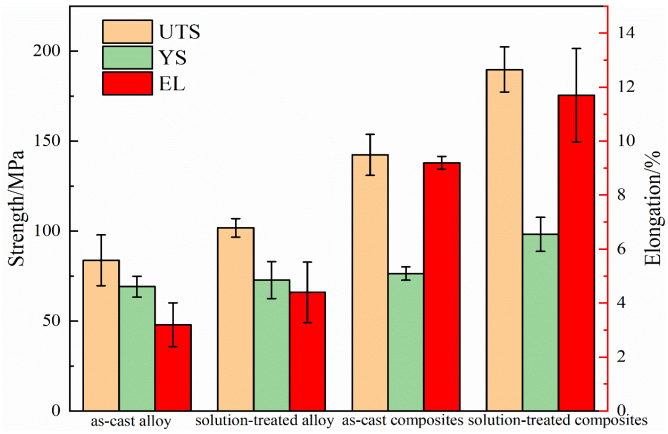

Figure 9. Mechanical properties of the alloys and the composites in as-cast state and after solution treatment.

Table 1. Mechanical properties of the alloys and the composites before and the after the solution treatment.

Materials	Hardness/HV	UTS/MPa	YS/MPa	EL/%
As-cast alloys	56.0 ± 5.9	83.8 ± 14.1	69.1 ± 5.8	3.2 ± 0.8
Solution-treated alloys	60.3 ± 5.7	101.8 ± 5.2	72.8 ± 3.7	4.4 ± 0.2
As-cast composites	113.0 ± 10.0	142.4 ± 11.4	76.4 ± 10.2	9.2 ± 1.1
Solution-treated composites	126.0 ± 9.0	189.8 ± 12.5	98.2 ± 9.5	11.7 ± 1.7

Both the as-cast and solution-treated composites exhibit superior strength and ductility over the monolithic alloys, and it is mainly due to the refinement of the Mg_2Si phase and α-Mg grains by the addition of dispersed TiB_2 particles, which was confirmed by the EDS mapping of Ti and B in our previous studies [25]. Figures 10 and 11 illustrate the grain structure of the as-cast alloys and the composites, and it can be seen from Figure 10a,c that the α-Mg grains in the composites was obviously refined, and the average grain size was decreased by 32.1% compared with the as-cast alloys, thereby contributing to the increase in hardness and strength based on grain refinement strengthening mechanism [37]. During the solution treatment, the α-Mg grain of both the alloys the composites grew slightly, and the size rise was 8.2% and 4.3%, respectively, indicating that the Mg_2Si phases and the TiB_2 particles inhibited grain growth to a certain extent during the solution treatment [38], but the refined Mg_2Si phases (green particles as shown in Figure 10d) together with the TiB_2 particles have more significant inhibition effect on the α-Mg grain growth compared with the coarse Mg_2Si phases (as shown in Figure 10b). Hence, the composites still owned super mechanical properties than the alloys even after the solution treatment.

The increase of hardness and strength of the composites and the alloys after the solution treatment is mainly due to the refined eutectic Mg_2Si particles, and the primary Mg_2Si particles with passivated corners effectively pined grain boundaries and hindered dislocation motion and improved the hardness and strength of the composites based on the load transfer mechanism [35]. In addition, the β-$Mg_{17}Al_{12}$ phases were dissolved into the α-Mg matrix (as shown in Figure 3b) to form the supersaturated solid solution, playing the role of solid solution strengthening [39]. The more significant strengthening effect of solution treatment for the composites in terms of hardness, UTS, and YS was mainly due to the branches of the eutectic Mg_2Si phases in the Mg-4Al-1.5Si alloys were partially dissolved into fragments, while the trunks remained long rod-like after the solution treatment, and the primary Mg_2Si phases were still coarse and irregular, as shown in Figure 12. On the other hand, the Mg_2Si phases in the composites were significantly refined by the addition of TiB_2 particles compared with that in the monolithic alloys, and the fine and discrete Mg_2Si blocks have more edges and corners, where Si concentration is higher and more prone to be preferentially dissolved [26,27], hence most of the Mg_2Si phases in the solution-treated

composites exhibited passivated particles or short rods. The addition of the TiB_2 particles may promote the Si diffusion during the solution treatment, hence contributing to a better modification effect on the Mg_2Si phases in the composites as shown in Figure 5b, but more investigations are needed in the future.

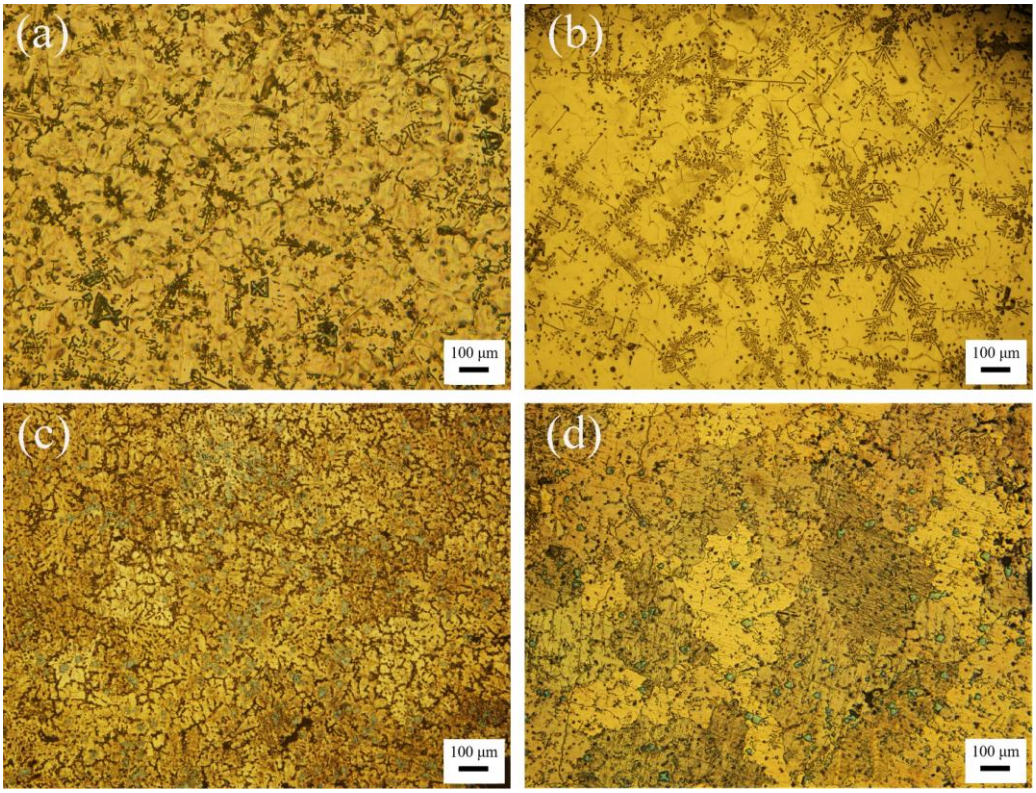

Figure 10. Optical micrographs showing the grain structure of the as-cast alloys (**a**); solution-treated alloys (**b**); as-cast composites (**c**); and solution-treated composites (**d**).

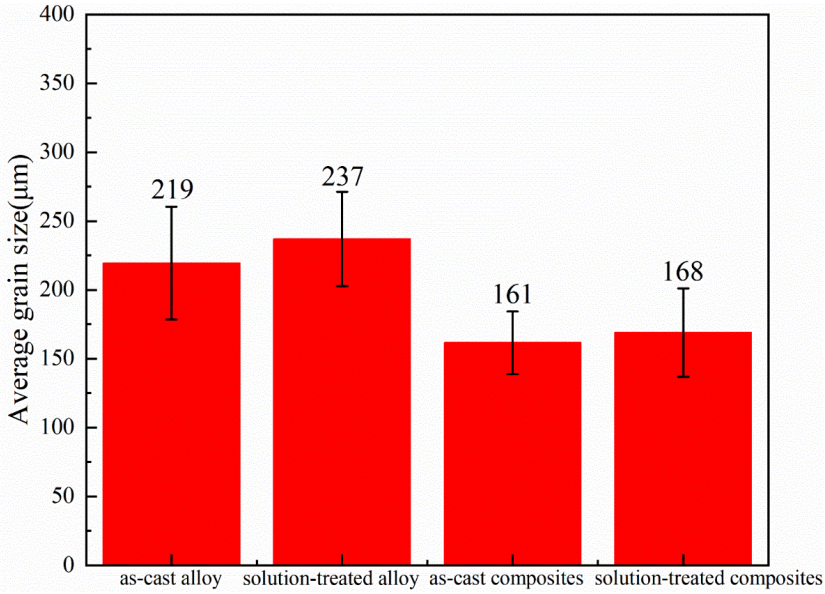

Figure 11. Average grain size of the alloys and the composites before and after solution treatment.

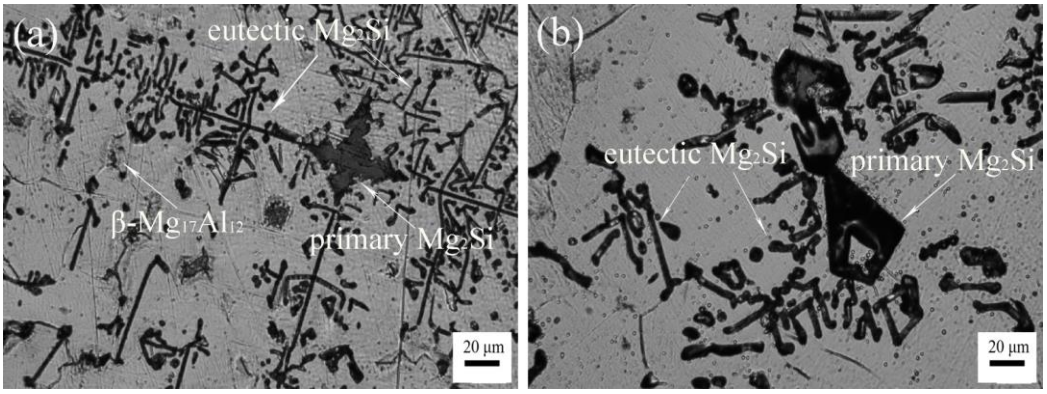

Figure 12. Optical micrographs of the as-cast alloys (**a**), and the solution-treated alloys (**b**).

Figure 13 illustrates the longitudinal section adjacent to the fracture surface of the composite and the monolithic alloy specimens in the as-cast state and after solution treatment. It is seen that the sharp corners of the primary Mg_2Si, and coarse eutectic Mg_2Si are preferential sites for initiation of cracks, and there are secondary cracks beneath the main cracks in the as-cast composite specimen (as shown in Figure 13a). However, no primary Mg_2Si and coarse eutectic Mg_2Si were found near the fracture surface of the solution-treated composites, and there are no secondary cracks beneath the main crack (as shown in Figure 13b). For the as-cast alloys, the coarse primary Mg_2Si and Chinese script eutectic Mg_2Si phases are preferential sites for initiation of cracks (as shown in Figure 13c), and there still exist coarse primary Mg_2Si and Chinese-script eutectic Mg_2Si near the fracture surface of the solution-treated alloys (as shown in Figure 13d), further confirming that the solution treatment has a better modification effect on the TiB_2/Mg-4Al-1.5Si composites compared with the monolithic Mg-4Al-1.5Si alloys.

It is reported that the local stress at the Mg_2Si/Mg interface is 2–4 times higher than that of the matrix due to the incompatibility between the Mg alloy matrix and Mg_2Si phases during the deformation process [9]. Hence, the Mg_2Si/Mg interface is usually the priority region of microcracks initiation and propagation. Thus, for the as-cast composites, during the tensile deformation, microcracks are preferentially initiated at the tips of eutectic Mg_2Si phases and the sharp corners of the primary Mg_2Si phases, where stress concentration was generated, and propagated along the Mg_2Si/Mg interface, hence causing a poor ductility of the as-cast composites. After the solution treatment, the brittle β-$Mg_{17}Al_{12}$ phase is completely dissolved into the matrix, the Chinese-script and short strip-like eutectic Mg_2Si phases were partially dissolved and spheroidized, and the sharp corners of the primary Mg_2Si phases were passivated, which is beneficial to relieving stress concentration and inhibiting crack initiation (as shown in Figure 13b) [26,28,40], hence the EL of the composites was improved significantly after the solution treatment. For the monolithic Mg-4Al-1.5Si alloys, there is no significant morphology change in both the eutectic Mg_2Si and primary Mg_2Si phases after the solution treatment, as shown in Figure 12. Considering that coarse Mg_2Si phases have poorer fracture strength and interfacial bonding compared with fine and regular-shaped Mg_2Si particles [41], hence the improvement in hardness, strength, and elongation is slight after the solution treatment, as shown in Table 1.

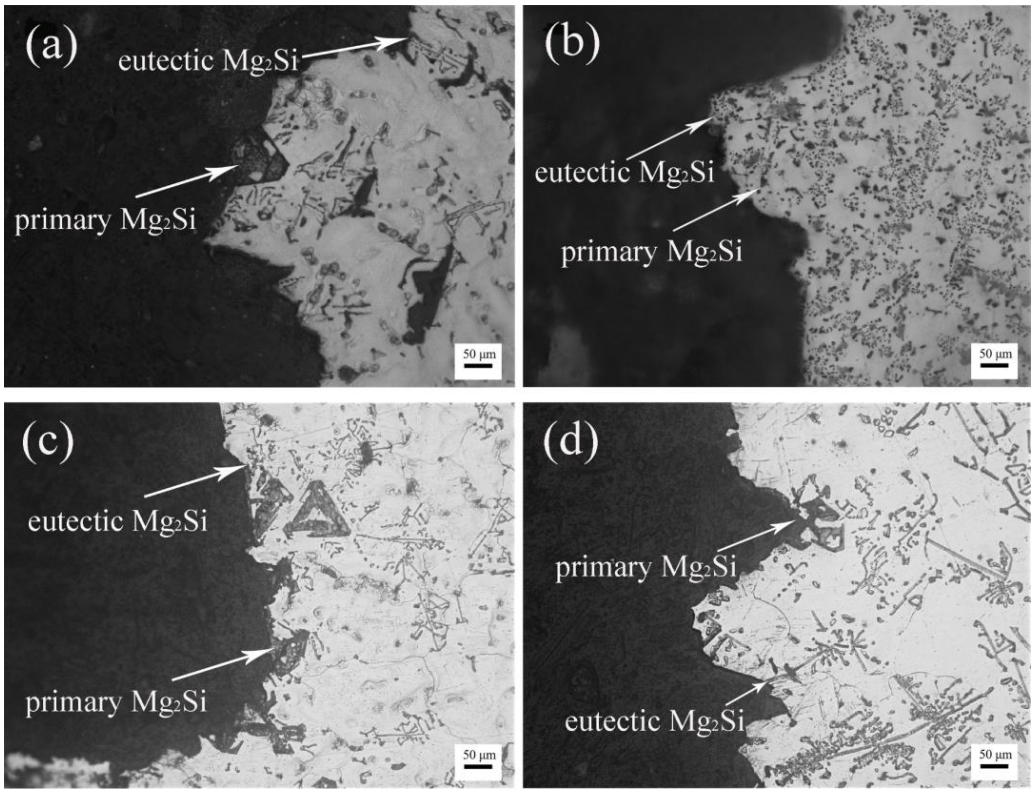

Figure 13. Side-views of fracture surfaces of the as-cast composites (**a**); the solution-treated composites (**b**); the as-cast alloys (**c**); and the solution-treated alloys (**d**).

4. Conclusions

(1) After the solution treatment at 420 °C × 24 h, partial branches of the eutectic Mg_2Si phases were decomposed into disconnected particles, and the sharp corners of the polygonal primary Mg_2Si phases were passivated due to Si diffusion at high temperature;
(2) After the solution treatment, the Vickers hardness, UTS, YS, and EL of the TiB_2/Mg-4Al-1.5Si composites were increased by 11.5%, 33.3%, 28.5%, and 27.2%, respectively compared with those of the as-cast composites;
(3) The solution treatment can be used to improve the strength and ductility of the TiB_2/Mg-4Al-1.5Si composites and the monolithic alloys, but the strengthening effect of the solution treatment is more significant for the composites in the hardness, UTS, and YS.

Author Contributions: Conceptualization, J.L. and X.C.; methodology, X.C.; software, X.C. and H.X.; validation, X.C. and S.Q.; formal analysis, X.C. and J.L.; investigation, X.C.; resources, W.W.; data curation, X.C.; writing-original draft preparation, X.C.; writing-review and editing, J.L.; visualization, X.C.; supervision, W.W. and J.L.; project administration, J.L.; funding acquisition, J.L. All authors have read and agreed to the published version of the manuscript.

Funding: National Nature Science Foundation of China (Program No. 52275377) and Natural Science Basic Research Plan in Shaanxi Province of China in 2022 (Program No. 2022JM-236).

Institutional Review Board Statement: Not applicable.

Informed Consent Statement: Not applicable.

Data Availability Statement: The data presented in this study are available upon request from the corresponding author.

Conflicts of Interest: The authors declare no conflict of interest.

References

1. Tan, J.; Ramakrishna, S. Applications of magnesium and its alloys: A review. *Appl. Sci.* **2021**, *11*, 6861. [CrossRef]
2. Xie, J.; Zhang, J.; You, Z.; Liu, S.; Guan, K.; Wu, R.; Wang, J.; Feng, J. Towards developing Mg alloys with simultaneously improved strength and corrosion resistance via RE alloying. *J. Magnes. Alloy.* **2021**, *9*, 41–56. [CrossRef]
3. Song, J.F.; Chen, J.; Xiong, X.M.; Peng, X.D.; Chen, D.L.; Pan, F.S. Research advances of magnesium and magnesium alloys worldwide in 2021. *J. Magnes. Alloy.* **2022**, *10*, 863–898. [CrossRef]
4. Zengin, H.; Turen, Y.; Elen, L.A. Comparative study on microstructure, mechanical and tribological properties of A4, AE41, AS41 and AJ41 magnesium alloys. *J. Mater. Eng. Perform.* **2019**, *28*, 4647–4657. [CrossRef]
5. Wang, C.; Ma, A.; Sun, J.; Zhuo, X.; Huang, H.; Liu, H.; Yang, Z.; Jiang, J. Improving strength and ductility of a Mg-3.7Al-1.8Ca-0.4Mn alloy with refined and dispersed Al_2Ca particles by industrial-scale ECAP processing. *Metals* **2019**, *9*, 767. [CrossRef]
6. Zhang, X.P.; Wang, H.X.; Bian, L.P.; Zhang, S.X.; Zhuang, Y.P.; Cheng, W.L.; Liang, W. Microstructure evolution and mechanical properties of Mg-9Al-1Si-1SiC composites processed by multi-pass equal-channel angular pressing at various temperatures. *Int. J. Miner. Metall. Mater.* **2021**, *28*, 1966–1975. [CrossRef]
7. Xu, T.; Yang, Y.; Peng, X.; Song, J.; Pan, F. Overview of advancement and development trend on magnesium alloy. *J. Magnes. Alloy.* **2019**, *7*, 536–544. [CrossRef]
8. Wang, F.; Xiao, W.; Liu, M.; Chen, J.; Li, X.; Xi, J.; Ma, C. Effects of alloying composition on the microstructures and mechanical properties of Mg-Al-Zn-Ca-RE magnesium alloy. *Vacuum* **2019**, *159*, 400–409. [CrossRef]
9. Li, P.B.; Yang, H.; Tan, W.T.; Gao, M.M. Effect of in situ Mg_2Si_p contents on microstructure and mechanical properties of Mg_2Si_p/AZ91D composites. *J. Mater. Sci.* **2021**, *56*, 6799–6813. [CrossRef]
10. Nakata, T.; Xu, C.; Sakai, T.; Miyamoto, T.; Liao, J.; Kamado, S. Effect of Si content on microstructures, tensile properties, and creep properties in a cast Mg-6Al-0.4Mn-2Ca(wt%) alloy. *Mater. Sci. Eng. A* **2020**, *776*, 139018. [CrossRef]
11. Zhang, Z.; Wang, H.; Wang, Z.; Li, H.; Li, Z.; Zheng, L.; Cheng, W. Enhanced mechanical properties of ECAPed Mg-9Al-1Si alloy by a two-stage pretreatment. *JOM* **2019**, *71*, 2178–2186. [CrossRef]
12. Seth, P.P.; Parkash, O.; Kumar, D. Structure and mechanical behavior of in situ developed Mg_2Si phase in magnesium and aluminum alloys-A review. *RSC Adv.* **2020**, *10*, 37327–37345. [CrossRef] [PubMed]
13. Hu, T.; Wang, F.; Zheng, R.X.; Xiao, W.L.; Li, Y.; Lyu, S.Y.; Ma, C.L. Effects of B and Sn additions on the microstructure and mechanical property of Mg-3Al-1Si alloy. *J. Alloys Compd.* **2019**, *796*, 1–8. [CrossRef]
14. Han, W.; Li, K.; Hu, F.; Li, Y.; Tang, B. Microstructure and mechanical properties of Mg-2.5Si-xCe in-situ particle reinforced composites prepared by rapid solidification process. *Results Phys.* **2019**, *15*, 102509. [CrossRef]
15. Chen, X.R.; Yin, Z.Y.; Le, Q.C.; Ning, S.C.; Yu, F.X. The microstructure refinement and strength enhancement of Mg-Al-Si alloy subjected by alternating-frequency ultrasonic melt treatment. *Int. J. Metal Cast.* **2022**, *16*, 474–480. [CrossRef]
16. Zhang, X.P.; Zhang, Z.Y.; Wang, H.X.; Zhuang, Y.P.; Wang, L.F.; Cheng, W.L.; Liang, W. Synergistic effect of broken Mg_2Si and sub-micron $Mg_{17}Al_{12}$ induced by EX-ECAP on the strength and ductility of deformed Mg-4Al-1Si-1Gd alloy. *J. Mater. Res. Technol.* **2020**, *9*, 4230–4240. [CrossRef]
17. Dong, Y.X.; Xiao, P.; Gao, Y.M.; Zhao, Q.Q.; Yang, H.C. Microstructure refinement and mechanical properties of eutectic Mg_2Si reinforced Mg matrix composites containing Sr element. *J. Mater. Res. Technol.* **2022**, *17*, 2614–2623. [CrossRef]
18. Lotfpour, M.; Bahmani, A.; Mirzadeh, H.; Emamy, M.; Malekan, M.; Kim, W.J.; Taghizadeh, M.; Afsharnaderi, A. Effect of microalloying by Ca on the microstructure and mechanical properties of as-cast and wrought Mg-Mg_2Si composites. *Mater. Sci. Eng. A* **2021**, *820*, 141574. [CrossRef]
19. Xiao, P.; Gao, Y.; Yang, C.; Dong, Y.; Huang, X.; Wang, Y.; Yang, S. Effect of Sb doping on microstructure, mechanical and electronic properties of Mg_2Si in Mg_2Si/AZ91 composites by experimental investigation and first-principles calculation. *J. Alloys Compd.* **2022**, *902*, 163859. [CrossRef]
20. Ganesh, M.R.S.; Reghunath, N.J.; Levin, M.; Prasad, A.; Doondi, S.; Shankar, K.V. Strontium in Al-Si-Mg alloy: A review. *Met. Mater. Int.* **2022**, *28*, 1–40. [CrossRef]
21. Sun, J.; Li, C.; Liu, X.; Yu, L.; Li, H.; Liu, Y. Investigation on AlP as the heterogeneous nucleus of Mg_2Si in Al-Mg_2Si alloys by experimental observation and first-principles calculation. *Results Phys.* **2018**, *8*, 146–152. [CrossRef]
22. Du, R.; Du, Y.; Li, F.; Zhang, D.C.; Wu, S.S.; Lü, S.L. Effect of in-situ TiB_2 particles on microstructure and mechanical properties of Mg_2Si/Al composites. *J. Alloys Compd.* **2019**, *776*, 536–542. [CrossRef]
23. Snopinski, P.; Krol, M.; Wrobel, T.; Matus, K.; Wozniak, A.; Tanski, T.; Palcek, P. Effects of modifying the hypoeutectic $AlMg_5Si_2Mn$ alloy via addition of $Al_{10}Sr$ and/or Al_5TiB. *Arch. Civ. Mech. Eng.* **2021**, *21*, 2. [CrossRef]
24. Kim, B.; Hwang, J.; Park, Y.H.; Lee, Y.C. Microstructural improvement of eutectic Al + Mg_2Si phases on Al-Zn-Si-Mg cast alloy with TiB_2 particles additions. *Metals* **2021**, *14*, 2902. [CrossRef] [PubMed]
25. Wang, W.X.; Chen, X.G.; Liu, J.; Liu, D.C.; Liu, Z.Z.; Li, W.Z.; He, N. Effects of TiB_2 nanoparticles and ultrasonic vibration on the mechanical properties of an Mg-4Al-1.5Si alloy. *J. Alloys Compd.* **2022**, *912*, 165213. [CrossRef]
26. Yu, H.C.; Wang, H.Y.; Chen, L.; Zha, M.; Wang, C.; Li, C.; Jiang, Q.C. Spheroidization of primary Mg_2Si in Al-20Mg2Si-4.5Cu alloy modified with Ca and Sb during T6 heat treatment process. *Mater. Sci. Eng. A* **2017**, *685*, 31–38. [CrossRef]
27. Jiang, W.Q.; Xu, X.F.; Zhao, Y.G.; Wang, Z.; Wu, C.; Pan, D.; Meng, Z.Y. Effect of the addition of Sr modifier in different conditions on microstructure and mechanical properties of T6 treated Al-Mg_2Si in-situ composite. *Mater. Sci. Eng. A* **2018**, *721*, 263–273. [CrossRef]

28. Chong, X.Y.; Jiang, W.Q.; Zhao, Y.G.; Xu, X.F.; Pan, D.; Wang, Y.T.; Wang, Z. High performance of T6-treated Al-15Mg2Si-3Cu composite reinforced with spherical primary Mg_2Si after the co-modification of Bi+Sr. *Adv. Eng. Mater.* **2019**, *21*, 1801119. [CrossRef]
29. Lv, J.; Dong, H.; Fan, L.; Yu, W.; Li, L. Effects of Bi-Sb addition and solution treatment on microstructures and mechanical properties of Al-20 wt.% Mg_2Si composites. *J. Mater. Eng. Perform.* **2019**, *28*, 3105–3114. [CrossRef]
30. Li, C.; Sun, J.; Li, Z.; Gao, Z.; Liu, Y.; Yu, L.; Li, H. Microstructure and corrosion behavior of Al-10%Mg_2Si cast alloy after heat treatment. *Mater. Charact.* **2016**, *122*, 142–147. [CrossRef]
31. Li, Z.; Li, C.; Liu, Y.; Yu, L.; Guo, Q.; Li, H. Effect of heat treatment on microstructure and mechanical property of Al-10%Mg_2Si alloy. *J. Alloys Compd.* **2016**, *663*, 16–19. [CrossRef]
32. Lekatou, A.G.; Poulia, A.; Mavros, H.; Karantzalis, A.E. Thermal treatment, sliding wear and saline corrosion of Al in situ reinforced with Mg_2Si and Ex situ reinforced with TiC particles. *J. Mater. Eng. Perform.* **2018**, *27*, 5030–5039. [CrossRef]
33. Xu, K.; Wang, J.J.; Zhang, S.Q. Effect of heat treatment on the microstructure and properties of in-situ Mg_2Si reinforced hypereutectic Al-18%Si matrix composites. *Mater. Res. Express.* **2020**, *7*, 086515. [CrossRef]
34. Wang, B.G.; Wang, X.; Zhou, J.X.; Zhang, G.F.; Liu, F. Effects of solution heat treatment on microstructure and mechanical properties of Mg-3Al-1Si-0.3Mn-xSr alloy. *Mater. Sci. Eng. A* **2014**, *618*, 210–218. [CrossRef]
35. Liu, J.A.; Song, D.; Zhang, L.R.; Yang, X.Z.; Zhu, X.Y.; Sun, W.B.; Chen, F.Y. Microstructure and compressive properties of solution heat-treated magnesium-Mg_2Si in-situ composite foams after complex modification. *J. Mater. Res. Technol.* **2021**, *15*, 3673–3682. [CrossRef]
36. Ghandvar, H.; Idris, M.H.; Ahmad, N. Effect of hot extrusion on microstructural evolution and tensile properties of Al-15%Mg_2Si-xGd in-situ composites. *J. Alloys Compd.* **2018**, *751*, 370–390. [CrossRef]
37. Xiao, P.; Gao, Y.M.; Xu, F.X.; Yang, S.S.; Li, B.; Li, Y.F.; Huang, Z.F.; Zheng, Q.L. An investigation on grain refinement mechanism of TiB_2 particulate reinforced AZ91 composites and its effect on mechanical properties. *J. Alloys Compd.* **2019**, *780*, 237–244. [CrossRef]
38. Geng, J.W.; Hong, T.R.; Shen, Y.W.; Liu, G.; Xia, C.J.; Chen, D.; Wang, M.L.; Wang, H.W. Microstructural stability of in-situ TiB_2/Al composite during solution treatment. *Mater. Charact.* **2017**, *124*, 50–57. [CrossRef]
39. Zhang, C.Y.; Li, Z.R.; Ye, Y.S.; Yuan, Y.L.; Fang, D.; Wu, H.H.; Li, W.Z. Interaction of nanoparticles and dislocations with $Mg_{17}Al_{12}$ precipitates in n-SiC_p/AZ91D magnesium matrix nanocomposites. *J. Alloys Compd.* **2020**, *815*, 152416. [CrossRef]
40. Ghandvar, H.; Bakar, T.A.A.; Idris, M.H. Influence of solution heat treatment on microstructure and tensile properties of Gd-treated Al-15% Mg_2Si in-Situ composites. *J. Appl. Sci. Eng.* **2021**, *25*, 521–528. [CrossRef]
41. Jin, Y.L.; Fang, H.Z.; Wang, S.; Chen, R.R.; Su, Y.Q.; Guo, J.J. Effects of Eu modification and heat treatment on microstructure and mechanical properties of hypereutectic Al-Mg_2Si composites. *Mater. Sci. Eng. A* **2022**, *831*, 142227. [CrossRef]